International Journal of Multiphase Flow 35 (2009) 335–348

Contents lists available at ScienceDirect

International Journal of Multiphase Flow

journal homepage: www.elsevier.com/locate/ijmulflow

Investigation of flow development of co-current gas–liquid vertical slug flow

R. Kaji [a], B.J. Azzopardi [a,*], D. Lucas [b]

[a] School of Chemical and Environmental Engineering, University of Nottingham, University Park, Nottingham NG7 2RD, UK
[b] Forschungszentrum Dresden-Rossendorf e.V., Institute of Safety Research, P.O.B. 510 119, D-01314 Dresden, Germany

ARTICLE INFO

Article history:
Received 28 November 2007
Received in revised form 14 August 2008
Accepted 18 January 2009
Available online 26 February 2009

ABSTRACT

Void fraction, Taylor bubble and liquid slug lengths, and slug frequency are parameters essential to any description of the structure of slug flow. In the present study, these parameters were extracted from the time series of cross-sectionally averaged void fraction obtained from two vertical facilities having similar internal pipe diameter but significantly different axial lengths; 51.2 mm/3.5 m and 52.3 mm/9 m. In order to study slug flow, the flow rates for which it occurred were first identified. To investigate the effect of flow development on slug characteristics measurements were carried out at several axial locations from the mixing section for both facilities. For slug frequency, a new correlation including the effect of the axial length has been proposed and assessed using previously published data.

1. Introduction

Slug flow in vertical pipes occurs in equipment employed in several industries, e.g., risers in hydrocarbon production; air-lift pumps; heat exchangers; evaporators and emergency core cooling for nuclear reactors. In oil and gas pipelines, detailed knowledge of the flow structure is important for the design of downstream separators which can be exposed to periodical impacts. Slug flow has a very clear periodic structure and consists of large bubbles whose sizes are almost equal to the pipe diameter (usually called Taylor bubbles) and liquid slugs containing small bubbles. Extensive detailed investigations of these bubbles and slugs have been carried out in the past and several physically based models have been proposed for fully developed flow (Fernandes et al., 1983; Sylvester, 1987; Barnea and Ullmann, 2004). An extensive review of the then available models was reported by Fabre and Liné (1992).

Obviously, in any study of slug flow, it is first necessary to establish at which flow rates that flow pattern will occur. Consequently, methods to identify the occurrence of flow patterns and their transitions were selected, tested and used.

Fig. 1 shows a schematic description of slug flow. Since Taylor bubbles move faster than the liquid slugs, a portion of liquid from the preceding slug transfers to the subsequent slug as a free falling film surrounding the bubbles. The bubble velocity can be obtained using the average of the liquid slug velocity and the bubble rise velocity, u_b (Nicklin et al., 1962). This is given by

$$u_b = C_0(u_{gs} + u_{ls}) + 0.35\sqrt{gD_t}. \quad (1)$$

C_0 is a parameter which varies with the liquid velocity and pipe diameter. u_{gs} and u_{ls} are the superficial velocities gas and liquid, respectively, g is the gravitational acceleration and D_t is the pipe diameter. For the case of turbulent flow, $C_0 = 1.2$ is commonly used. Delfos et al. (2001) reported that bubble entrainment in liquid slugs depends strongly on the film flow surrounding Taylor bubbles since bubble entrainment occurs when the film flow plunges into the subsequent liquid slug. Some of these bubbles re-coalesce with the tail of the bubble due to a wake recirculation. This wake zone which consists of a cloud of bubbles is about 1–10 pipe diameters in length. This is followed by the far wake or low void fraction zone which extends down to the next Taylor bubble. The length of this region has been reported to be about 1–19 pipe diameters. Very close to the Taylor bubble tail Sekoguchi and Mori (1997) reported a liquid swelling zone whose length varies with 0.15–5 pipe diameters. However, most researchers have combined the liquid swelling zone with either Taylor bubble or the wake zones.

The majority of published work on slug frequency focused on pipes which are at or near horizontal. Zabaras (2000) assessed eight existing equations describing slug frequency using 399 points of air–water data from 0–11° and concluded that none of them gives satisfactory prediction. He developed a simple correlation based on physically based model proposed by Taitel and Dukler (1976). The result agrees within an accuracy of 60%. For vertical flow, however, no consolidated correlation is available so far. Legius et al. (1997) adapted the correlation by Heywood and Richardson (1979) for horizontal flow to their vertical flow data and obtained reasonable agreement.

These parameters might vary with the axial distances because the flow is still developing. There is no clear understanding how long does this axial distance need to be before it can be described as fully developed slug flow. At lower gas flow rates, Radovcich and Moissis (1962) suggested a model for bubble collision frequencies, reported the extremely high collision rate at void fraction >0.25 and concluded that the magnitude of this frequency which is associated

* Corresponding author. Tel.: +44 115 951 4160; fax: +44 115 951 4115.
E-mail address: barry.azzopardi@nottingham.ac.uk (B.J. Azzopardi).

0301-9322/$ - see front matter © 2009 Elsevier Ltd. All rights reserved.
doi:10.1016/j.ijmultiphaseflow.2009.01.004

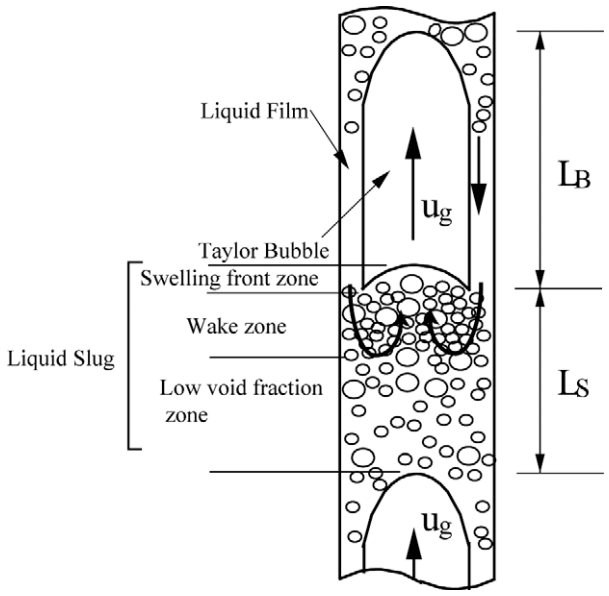

Fig. 1. The schematic model of slug flow.

with the bubble coalesce rate determined how quickly the flow pattern changed from bubbly to slug. Taitel et al. (1980) proposed a critical void fraction for this transition. Further investigation revealed that there was an effect of bubble size on the flow pattern transition (Liu, 1993; Song et al., 1995; Azzopardi, 2006). The importance of the interplay between local effects and bubble coalescence was pointed out by Lucas et al. (2003). In contrast, at higher gas flow rates, it has been reported that slug flow was forming from a churn-like flow lower in the pipe (Taitel et al. (1980)). This phenomenon occurs since the length of bubbles and slugs are short. Moissis and Griffith (1962) and Pinto and Campos (1996) investigated the interaction between two successive slugs and found that slug lengths greater than a minimum value are required for a stable state to be achieved. Previous studies on flow development include those of Brown et al. (1975) and Wolf et al. (2001) who investigated the flow development for annular flow and concluded that the order of 100 pipe diameters are necessary for the flow to be fully developed though for some parameters Brown et al. reported that 600+ diameters might be required. For slug flow, the velocity of Taylor bubble decreases and the Taylor bubble/liquid slug lengths increases along the pipe (van Hout et al. (2001)). However, short slugs were reported to exist at their furthest sensor, located about 7 m from inlet and from this it was inferred that occasional coalescence still occurs at this distance.

In the present study, the effect of development length on flow pattern and slug characteristics such as void fraction, Taylor bubble/slug length and frequency have been investigated using time series of cross-sectionally averaged void fraction obtained at several axial distances from the mixer using a wire-mesh sensor developed by Prasser et al. (1998, 2001). The contribution of the axial distance on flow pattern and slug characteristics is reported.

2. Experimental facilities

The data analysed in this study were obtained from two facilities called MTLoop and TOPFLOW, located at Forschungszentrum Dresden-Rossendorf (FZD), Germany. These are described below.

2.1. MTLoop

The MTLoop facility has a vertical test section consisting of a 51.2 mm internal diameter pipe, 3.5 m tall. The operational conditions can be air–water or steam–water flows at pressures up to 2.5 MPa. The gas and water flow rates were measured by using hot wire sensor and ultrasonic flow meter, respectively. Nineteen 0.8 mm diameter capillaries regularly distributed about the cross section were provided for gas injection. To avoid the asymmetric injection due to flow maldistribution, especially at low gas flow condition, capillaries were divided into 5 groups and each group was connected to an individual feed line. Void fractions were measured at 10 different axial locations (Dimensionless axial distances were 0.59, 1.56, 2.54, 4.49, 8.40, 16.2, 29.9, 39.6, 49.4 and 59.2 pipe diameters) by using a wire-mesh sensor to investigate the flow development. The conditions at which experiments were carried out were: liquid superficial velocity = 0–4.05 m/s and gas superfi-

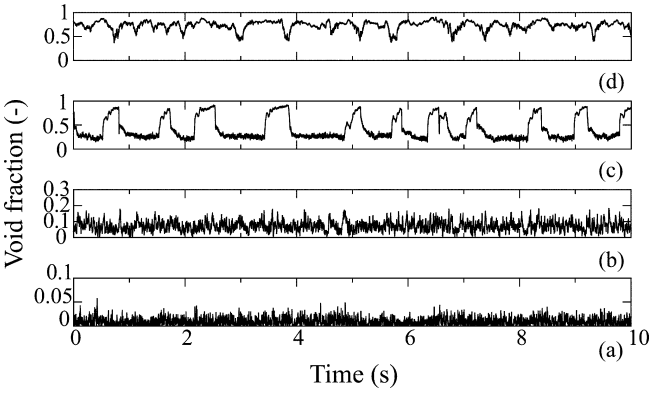

Fig. 2. Representative cross-sectionally averaged time series of void fraction from each flow pattern. (a) wall-peaking bubbly flow; (b) core-peaking bubbly flow, (c) slug flow and (d) churn flow.

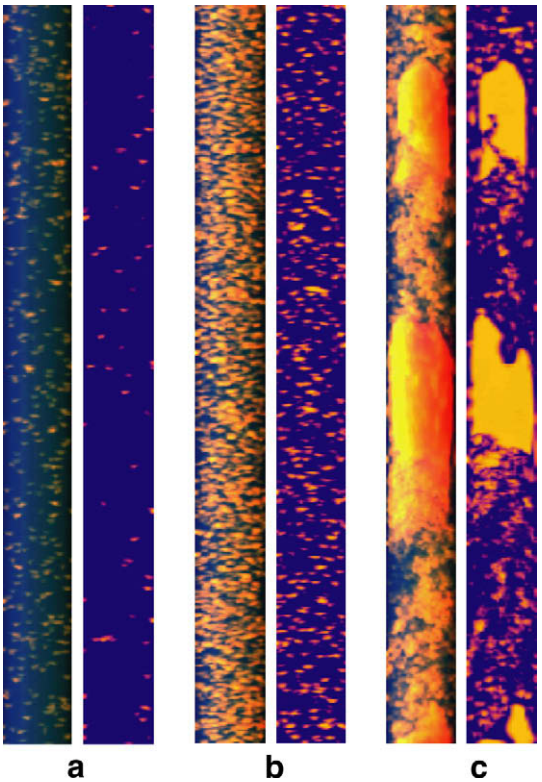

Fig. 3. Integral side view and data of local void fraction along a diameter. (a) wall-peaking bubbly flow, (b) core-peaking bubbly and (c) slug flow.

cial velocity = 0.0025–0.534 m/s. Details about these measurements are provided by Lucas et al. (2005).

2.2. TOPFLOW

The TOPFLOW facility has a vertical test section consisting of a 52.3 mm internal diameter pipe, 9 m tall. The facility can be operated with air–water or steam–water flow and can be pressurized up to 7 MPa. In the present air–water experiments, air was released to atmosphere from a separator vessel where two phase mixture was separated. The air was injected through eight 4 mm holes and its flow rate measured by hot wire volume meter (±1.5% accuracy) whilst the water was metered by standard nozzle meter with accuracy of ±1%. Void fractions were measured at 4 different positions using a wire mesh sensor. The dimensionless axial distances were 1.9, 30.6, 59.3 and 151.2 pipe diameters. The experimental conditions over which experiments were carried out were: liquid superficial velocity = 0–4 m/s and gas superficial velocity = 0.0025–19 m/s. Details on these measurements are described by Prasser et al. (2007).

For both the MTLoop and TOPFLOW experiments, measurements were carried out at only one axial position per run because the wire-mesh sensor affects the flow downstream of it; therefore, the same experiment conditions were repeated with the sensor at different positions.

2.3. Wire-mesh sensor

In both facilities, cross-sectionally resolved time-varying void fractions were obtained by using wire-mesh sensor reported by Prasser et al. (1998, 2001). The sensor consists of two parallel wire grids positioned orthogonally but offset by a small distance in the axial direction. One grid works as a transmitter the other as a receiver. By activating each wire successively, the current at each crossing point is detected. The local instantaneous void fractions are calculated from the measured conductivity between crossing points. If the process is iterated over all crossing points, a series of two dimensional data sets can be obtained. By reconstructing these sets in time sequence high speed visualisation can be

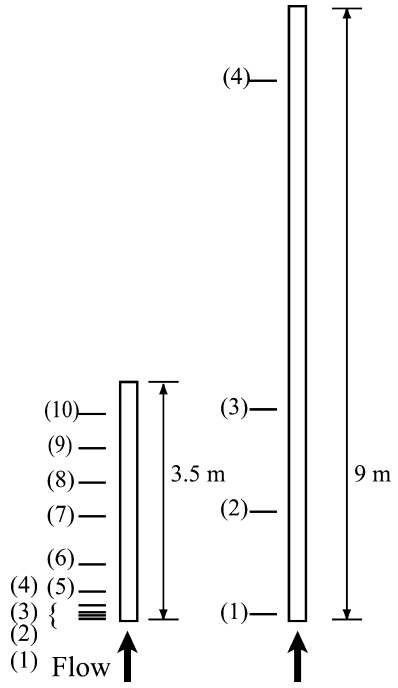

Fig. 5. The locations of the sensor for MTLOOP and TOPFLOW.

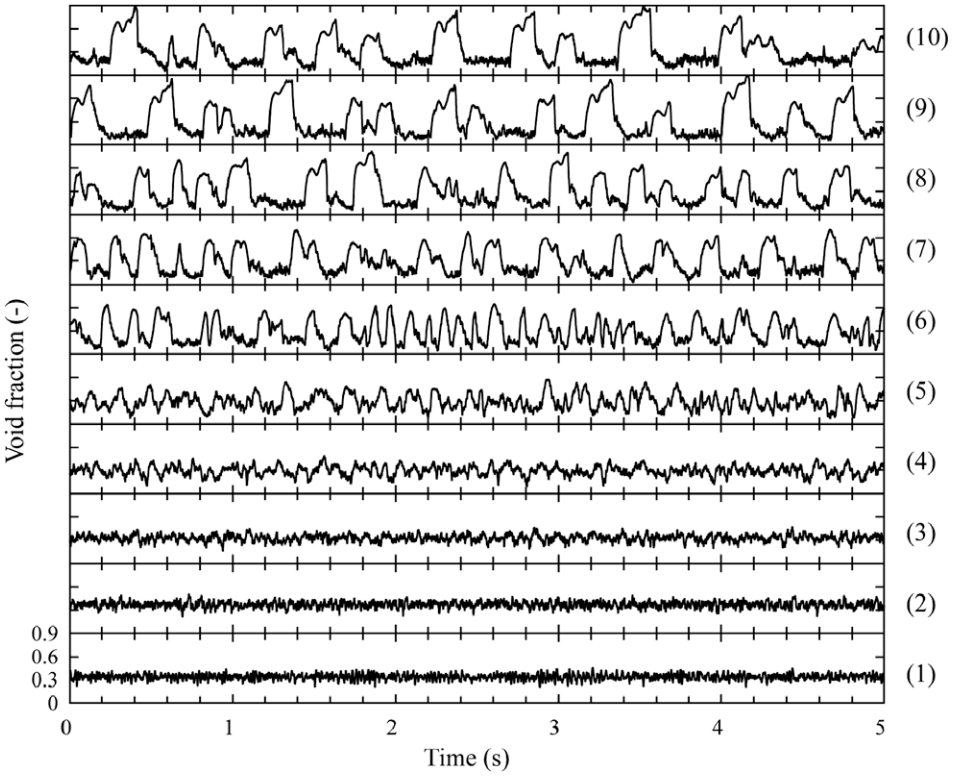

Fig. 4. Axial variation of time series void fraction (Liquid superficial velocity = 0.40 m/s; gas superficial velocity = 0.34 m/s, (1)–(10) refer to measurement locations as indicated in Fig. 5.

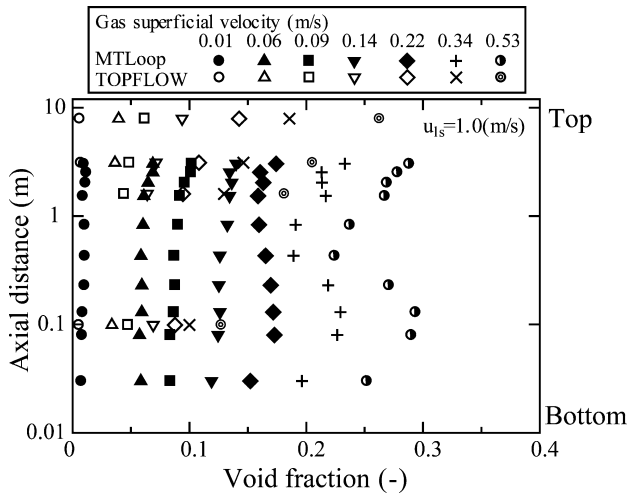

Fig. 6. Effect of gas flow rate on the axial variation of mean void fraction (Liquid superficial velocity = 1.0 m/s).

achieved. In addition, Prasser et al. (2001) reported that bubble size distribution information could be abstracted by using the bubble identification process. A 24 × 24 mesh with wires of 120 μm diameter was employed in the experiments reported here. The offset between the wire grids and the lateral distance between wires were 1.5 mm and 3 mm, respectively, and this determined the spatio/temporal resolution of the sensor. Data was acquired at the cross-section frequency of 2.5 kHz for 10 s. The output of the wire mesh sensors can be analysed at a number of levels. Here, the time series of the cross-sectionally averaged void fraction have been extracted and analysed to provide slug flow characteristics.

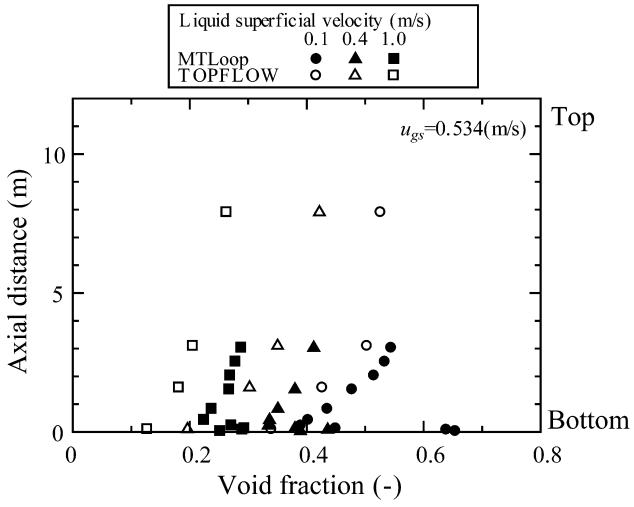

Fig. 7. Effect of liquid flow rate on the axial variation of mean void fraction (Gas superficial velocity = 0.534 m/s).

3. Results

3.1. Void fraction time series

Examples of time series of cross-sectionally averaged void fraction obtained from the TOPFLOW facility are shown in Figs. 2(a)–(d). These figures are representative signals from different flow patterns, i.e., wall peaking bubbly flow, core peaking bubbly flow, slug flow and churn flow. No annular flow was observed under the conditions of the present experiments. Fig. 3 shows integral side views, i.e., what would be seen if the pipe was transparent. It is created by integrating data along chords in the viewing direction. Also shown are the data from across a pipe diameter of local phase occurrence for each flow pattern. The y directions in these figures are not axial distance but the time history at one horizontal plane. Flow development is illustrated in Fig. 4 which shows the time

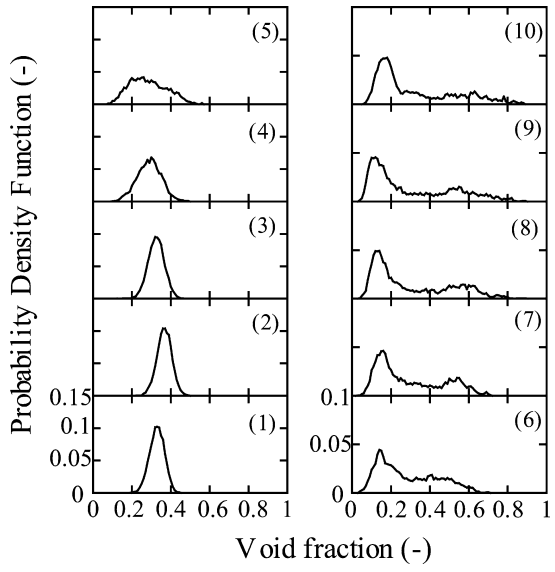

Fig. 9. Probability density function showing flow development along the axial distances (Liquid superficial velocity = 0.40 m/s, gas superficial velocity = 0.34 m/s; (1)–(10) corresponds to the measurement locations indicated in Fig. 5).

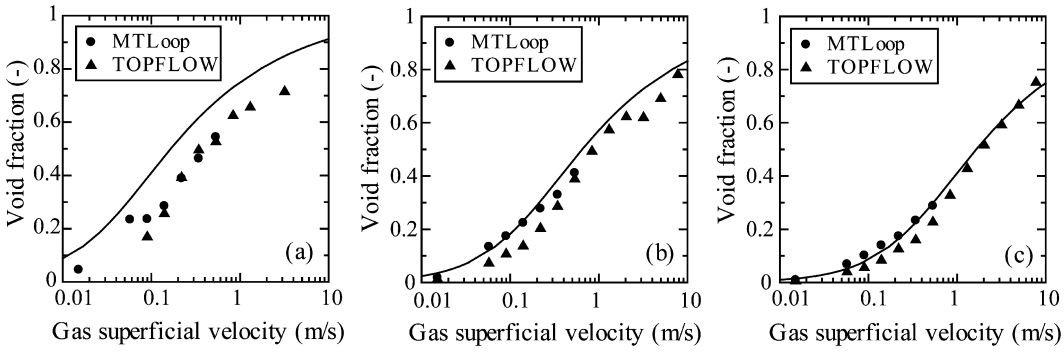

Fig. 8. Averaged void fraction versus gas superficial velocity for different liquid superficial velocities ((a) 0.1 m/s, (b) 0.4 m/s, and (c) 1.0 m/s). The lines are the predictions of the simple correlation by Chisholm (1972).

series of cross-sectionally averaged void fraction from different axial positions clearly illustrating the bubble to slug transition. Numbers indicates the position of the sensors shown in Fig. 5. It is clearly seen that flow development occurs along the pipe with bubbly flow in the lower part of the pipe and slug flow towards the top.

3.2. Averaged void fraction

Fig. 6 shows the effect of gas flow rate on the axial variation of mean void fraction at the liquid superficial velocity of 1.0 m/s. For the TOPFLOW data the void fraction increases systematically with the axial distance. In contrast, for the MTLoop data, there is a sudden increase of void fraction at the position very close to the inlet (Z/D_t <5) for some flow conditions, especially at high gas volume rates. Here, Z is the axial distance from the mixer and D_t is the pipe diameter. It is assumed that this is a combined effect caused the gas injection and radial redistribution of the bubbles. For the smallest distance from the injection the radial gas fraction profiles still show a pronounced maximum at those radial positions where the rings of capillaries are located. The gas is injected with high velocity. This and the high local void fraction cause high local gas velocities at this measuring position. Afterwards the bubbles redistribute over the cross section which is connected with a de-acceleration. The decreasing average gas velocity causes the increase of average void fraction. At the higher positions it is considered that the difference between the facilities is probably due to the gravitational pressure drop. Both have atmospheric pressure at the top and different heads of a two-phase mixture causes differences in void fraction lower down. It is important to recognise that there is a different local pressure at the same Z/D_t in MTLoop and TOPFLOW for the comparisons between both datasets.

Fig. 7 shows the effect of liquid flow rate on the axial variation of mean void fraction at the gas superficial velocity of 0.534 m/s. Obviously, the mean void fraction decreases with increasing liquid flow rate. The gradient of mean void fraction with axial distance also decreases with increasing liquid flow rate, especially near the inlet. It is considered that this effect is linked to the radial redistribution of the bubbles and the consequent differences in relative velocity between the phases. A further effect that causes differences in the axial direction is that of pressure drop which causes bubble to expand. However, this effect is rather small because the pressure gradient is higher at higher liquid superficial velocities. This should lead to a higher gradient of mean void fraction which is in contrast to the trend shown in Fig. 7.

The mean void fraction taken from the highest sensor is plotted in Fig. 8 against the gas superficial velocity at three different liquid superficial velocities. For reference, the simple empirical correlation based on a separated flow model proposed by Chisholm (1972) is also plotted. The correlation predicts the trends in the data correctly and gives better fits as the liquid flow rate is increased.

3.3. Probability density function

The Probability Density Functions (PDFs) of time varying properties of a gas/liquid flow have been shown to be useful and objective tools to identify flow patterns. Jones and Zuber (1975) suggested that flow pattern could be identified depending on the shape of PDF. More recently, Costigan and Whalley (1996) carried out the extensive work to link specific PDF signatures with six different flow patterns. In the present study, four signatures of the PDFs of cross-sectionally averaged void fraction times series are used for flow identification, i.e., single peak at low void fraction for bubbly flow, two-peaks for slug flow, single peak at high void fraction (all void fraction >0.8) for annular flow. Churn flow is identified the pattern between slug and annular flow, i.e., single peak at high void fraction with a widely distributed tail at lower void fraction. The PDFs corresponding to the void fraction time series in Fig. 4 are shown in Fig. 9. Flow pattern transition from bubbly to slug flow can clearly be seen to have occurred by station six.

The development of the flow along the pipe can be illustrated by considering the void fractions in the Taylor bubbles and slug regions. These can be obtained from the peaks of PDFs. Fig. 10a

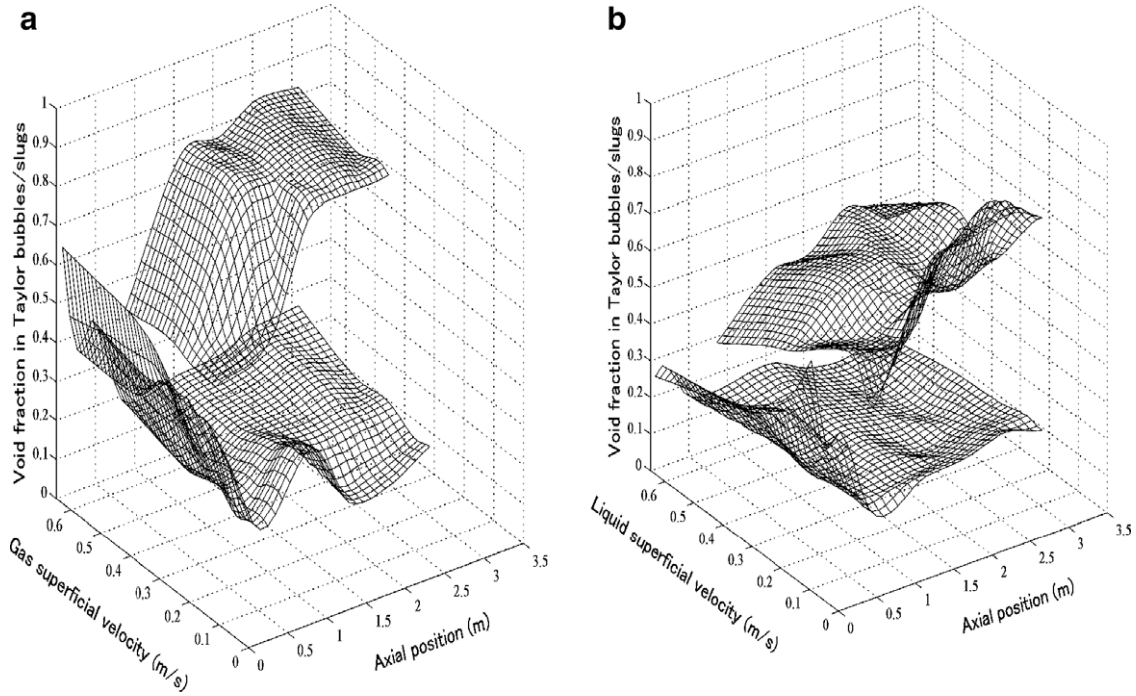

Fig. 10. Development of slug flow structure: (a) effect of different gas superficial velocities at liquid superficial velocity of 0.102 m/s; (b) effect of liquid superficial velocities at gas superficial velocity of 0.342 m/s.

shows data for a constant liquid superficial velocity of 0.102 m/s whilst Fig. 10b illustrates those data for a constant gas superficial velocity of 0.342 m/s. The upper and lower surfaces show void fraction in Taylor bubbles and liquid slugs, respectively. The smooth surfaces shown were obtained employing cubic interpolation of experimental information. In both figures, the upper surface does not occur at axial positions near the mixer. This is because the PDFs obtained at those positions are charactertised by a single peak indicating bubbly flow. The values from those single peaks decrease asymptotically as the flow develops and becomes slug flow. On the other hand, for the upper surface, the void fraction in the Taylor bubbles, initially increases along the pipe but then settles to steady values. The gap between the peaks becomes wider with the distance from the inlet. The void fraction in Taylor bubbles and liquid slugs tend to increase with increasing gas flowrates and decreasing liquid flowrates.

3.4. Bubble size distribution/radial gas volume fraction

Wire mesh sensors provide detailed information such as bubble size distribution and radial gas volume fraction. The bubble size distribution, p, employed is that based on gas volume fraction instead of the more usual one based on the bubble number density. It is defined as

$$p(D_b) = \frac{d(\varepsilon_{gb})}{d(D_b)}, \tag{2}$$

where $d\varepsilon_{gb}$ is the portion of the void fraction contained in bubbles of diameters between D_b and $D_b + dD_b$. Bubble sizes were determined assuming that all bubbles are spherical. Figs. 11(a) and (b) show examples of PDFs, bubble size distributions and the variation of gas volume fractions along a pipe radius which have been obtained from the TOPFLOW data. One set was taken at near bubble slug transition regime and the other within the slug flow regime. Lucas et al. (2005) identified slug flow as occurring when the bubble size becomes larger than the pipe diameter. From these figures, the conditions at which slug flow occurs, identified using Probability Distribution Functions, is in good agreement with those from bubble diameter. For both cases core-peaking bubble distribution are seen with the peak of radial profile of gas volume fraction becoming flattened as flow travels downstream.

3.5. Power spectrum density

Dominant frequencies can be obtained by using Power Spectrum Density functions (PSD). This is estimated by using Fourier transform of the auto covariance function of the void fraction time series. From the time series, the auto covariance function at an arbitrary time delay $R_{xx}(k\Delta\tau)$ is defined as:

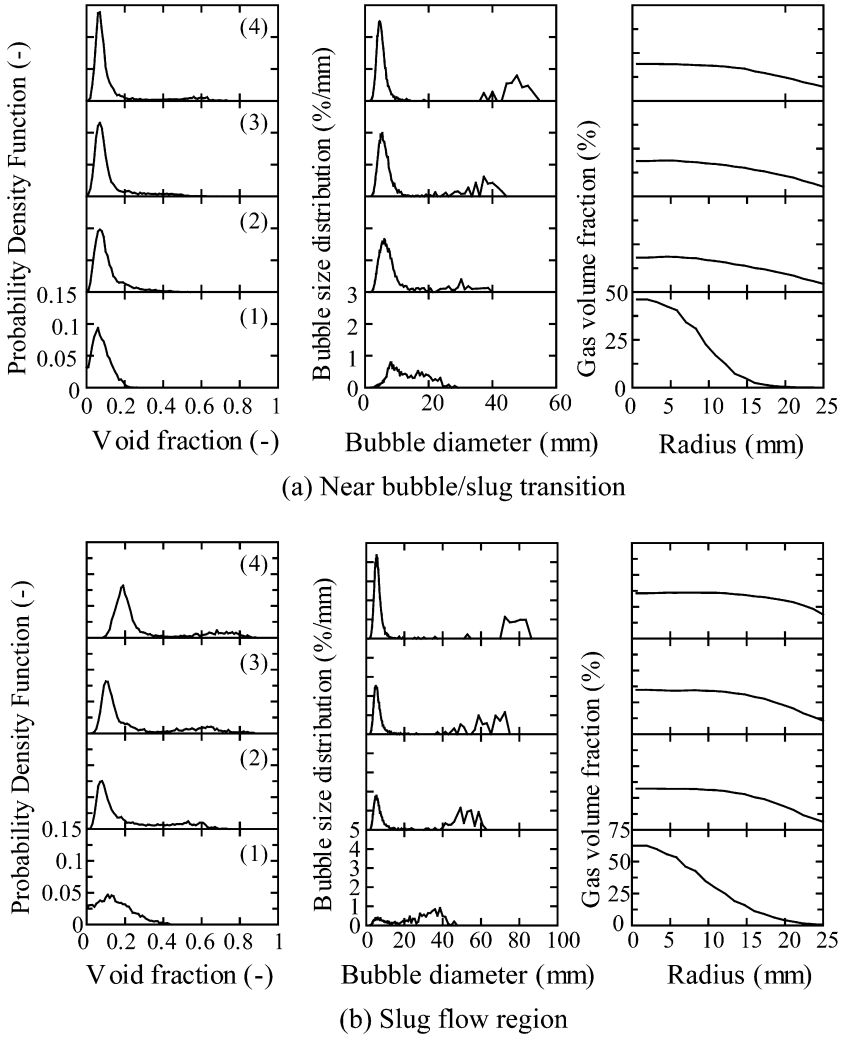

Fig. 11. Probability density function, bubble size distribution and radial gas volume fraction ((a) liquid superficial velocity = 0.40 m/s, gas superficial velocity = 0.14 m/s; (b) liquid superficial velocity = 0.40 m/s, gas superficial velocity = 0.34 m/s; (1)–(4) correspond to the measurement locations shown in Fig. 5).

$$R_{xx}(k\Delta\tau) = \frac{1}{T-\tau}\int_0^{T-\tau} (\varepsilon_g(t) - \bar{\varepsilon}_g)(\varepsilon_g(t+k\Delta\tau) - \bar{\varepsilon}_g)dt, \quad (3)$$

where t is time, T is the sampling duration, $\Delta\tau$ is the resolution of time delay, τ is the interrogation time delay and $\bar{\varepsilon}_g$ is the averaged void fraction in the whole time series. The power spectrum density function is then obtained from:

$$P_{xx}(f) = \sum_{k=-\infty}^{\infty} R_{xx}(k\Delta\tau)w(k\Delta\tau)\exp(i2\pi fk\Delta\tau). \quad (4)$$

$w(k\Delta\tau)$ is a windowing function which is introduced to suppress the spectrum leakage that mainly appears as the side lobes at high frequency end of the spectrum. Here f is the frequency. In the present study, following simple cosine window function was employed:

$$w(k\Delta\tau) = \cos\left(\frac{\pi k\Delta\tau}{2\cdot\tau}\right). \quad (5)$$

Since auto covariance has no phase lag, discrete cosine Fourier transform can be applied:

$$P_{xx}(f) = \Delta\tau\left(\frac{1}{2}R_{xx}(0) + \sum_{k=1}^{\tau/\Delta\tau-1} R_{xx}(k\Delta\tau)w(k\Delta\tau)\cos(2\pi fk\Delta\tau)\right). \quad (6)$$

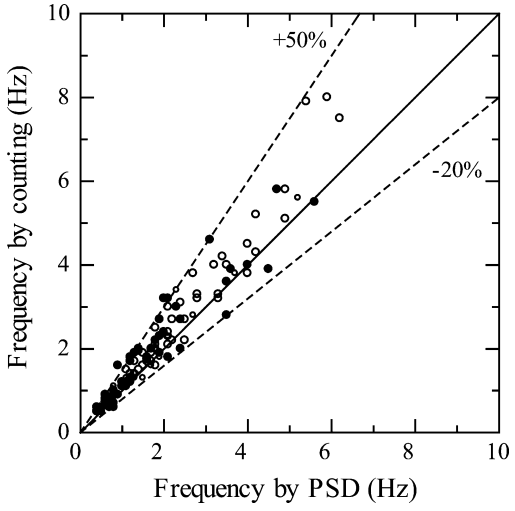

Fig. 12. Slug frequencies obtained from the counting method and the Power Spectrum Density (Open symbol: MTLoop, Filled symbol: TOPFLOW).

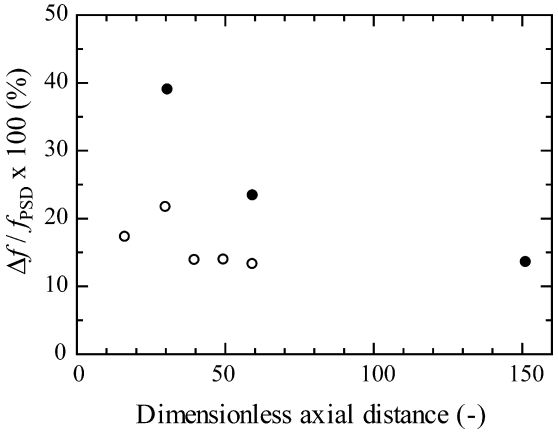

Fig. 13. Difference in frequencies from the PSD and the counting method against axial distance (open symbol: MTLoop, filled symbol: TOPFLOW).

To verify the results, dominant frequency were also obtained by simply counting the number of slug units in a fixed time. Fig. 12 shows the frequency results in slug region obtained from the PSD and the counting method. In calculating the PSDs, interrogation time delay = 1 s was employed. However, it was found that the results obtained were not sensitive to this time. From the figure, it is found that slightly lower frequencies were determined from the PSD than the counting method. For the present data, the differences lie in the range of −20% to +50%.

Fig. 13 shows the differences in frequency from the PSD and the counting method against axial distance. In both facilities the difference decreases with increasing axial distance. This indicates that the slug structure becomes more periodic as flow travels downstream.

4. Discussion

4.1. Flow pattern maps

For each condition flow patterns have been identified from its PDF. Fig. 14 shows the flow pattern map from both experiments based on data from the sensor furthest from the inlet. It is seen that the correlation by Lucas et al. (2005), which is given in Eq. (7),

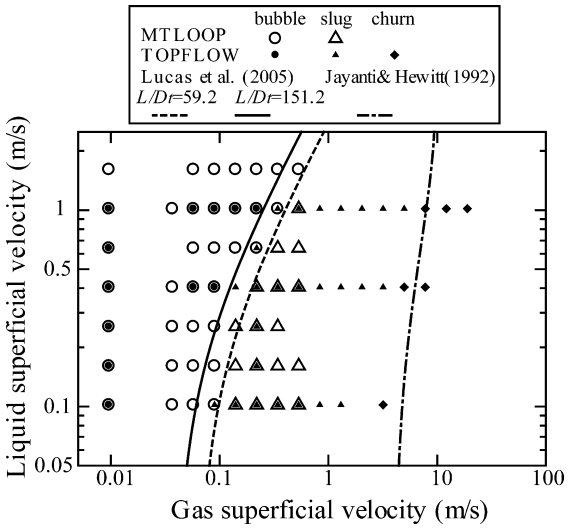

Fig. 14. Flow pattern map showing transition lines.

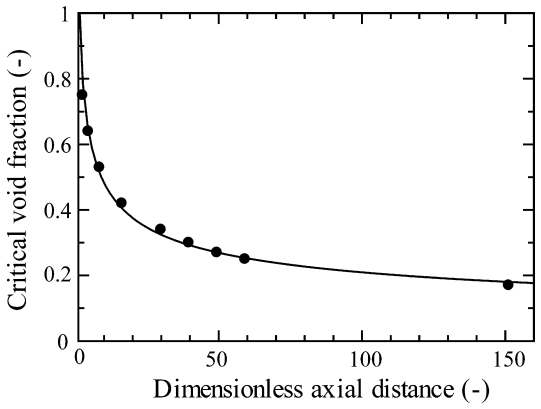

Fig. 15. Critical void fraction against dimensionless axial distance.

based on the result from the MTLoop facility (51.2 mm) also predicts successfully for the longer length of $L/D_t = 151.2$.

$$u_{ls} = 3.0u_{gs}\sqrt{\frac{L/D_t - 1}{60}} - 1.15\left[\frac{g(\rho_l - \rho_g)\sigma}{\rho_l^2}\right]^{0.25} \quad (7)$$

where ρ_g and ρ_l are the densities of gas and liquid and σ is the surface tension. The model by Taitel et al. (1980) links the bubble to slug transition to a critical void fraction for which they proposed a constant value of 0.25. Song et al. (1995) suggested that this critical void fraction might not be a constant but that it might depend on the bubble size. Azzopardi (2006) brought together the data from several sources which show that the critical void fraction depends on a bubble size made dimensionless by the pipe diameter. Data from Song et al. (1995) in a 39 mm pipe, Cheng et al. (2002) in a 29 mm pipe and Guet et al. (2002) in a 72 mm pipe were used in this exercise which showed that the critical void fraction decreases linearly with increasing dimensionless bubble size. If the concept of a critical void fraction was applied to the data from different axial positions, the critical void fraction would have to decreases exponentially with the axial distance (Fig. 15). This indicates that higher gas fraction is necessary to form slug flow near the inlet. It was noted that very similar bubble sizes were measured for equivalent runs on the MTLoop and TOPFLOW facilities. For slug to churn flow transition the model by Jayanti and Hewitt (1992) show trends similar to those seen in the experimental data but the predicted gas superficial velocities are slightly higher.

4.2. Statistical analysis of flow pattern identification

The data considered in the present work have been examined so as to identify a more objective method of flow pattern identification. Fig. 16(a)–(c) shows how statistical parameters such as the Standard Deviation, Skewness and Kurtosis of the cross-sectionally averaged void fraction vary with the gas superficial velocity. These statistical functions are defined in the Appendix. Symbols indicate the flow pattern and the lines trace the loci at constant liquid flow rates. From these figures it can be deduced that the Standard Deviation is a useful tool to identify slug flow. A Standard Deviation of 0.1 corresponds to the transition from bubbly to slug flow and to

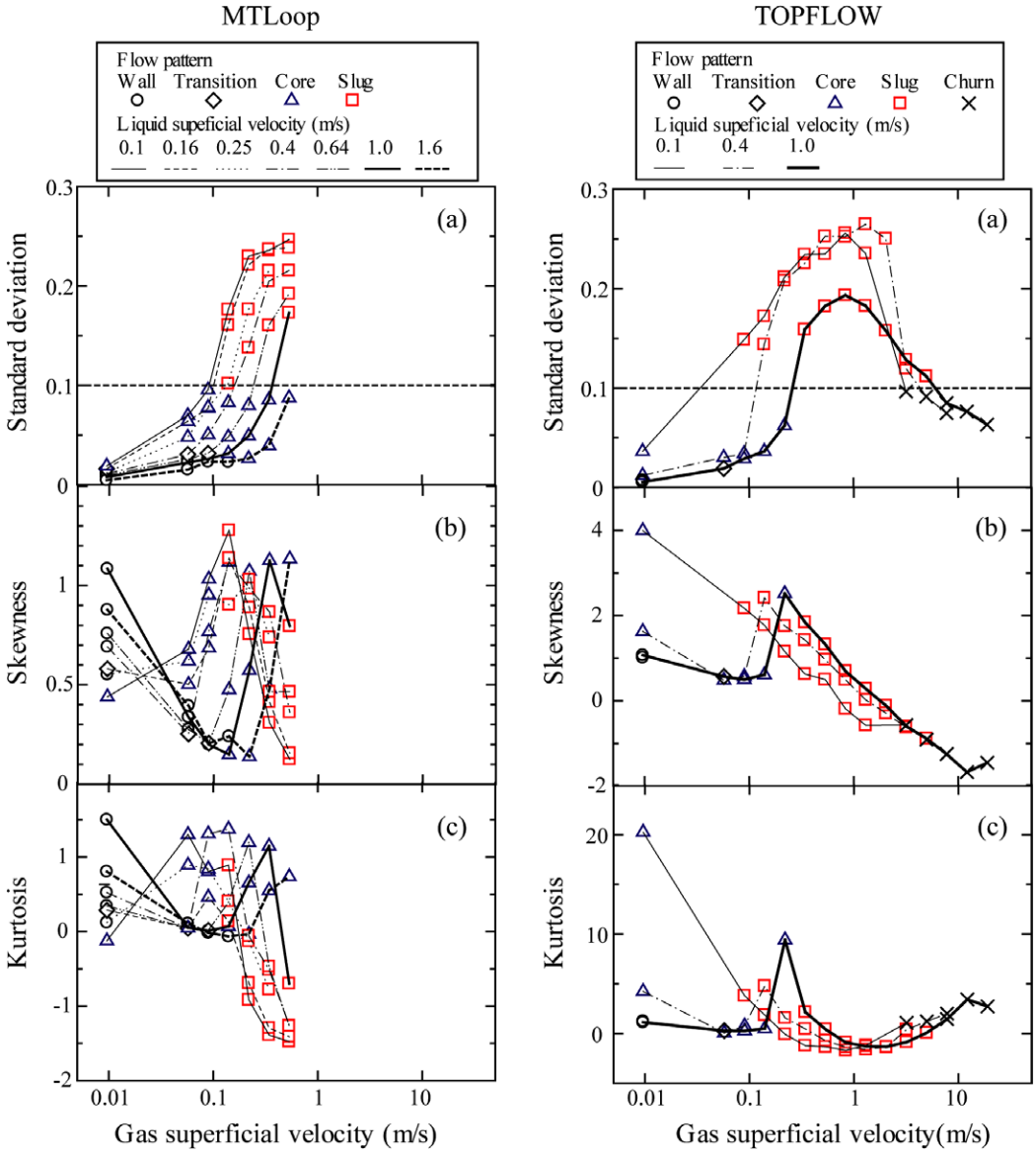

Fig. 16. Flow pattern of MTLoop and TOPFLOW facilities with (a) Standard Deviation (b) Skewness (c) Kurtosis (flow pattern shows core-peaking and wall-peaking bubbly flow and their transition, slug flow and churn flow). The dashed line in (a) is the suggested threshold.

that for slug to churn flow, i.e., Standard Deviations >0.1 occur for slug flow whilst those for <0.1 are found for bubble and churn flow pattern. The variation of other statistical parameters, i.e., Skewness and Kurtosis, did not appear to be so clearly linked to flow pattern transition.

4.3. Slug unit structure

The values of the parameters describing slug structure were extracted for those conditions determined as slug flow in the previous section. The data used were those at the sensor furthest from the inlet, i.e., 3 m in MTLoop and 8 m in TOPFLOW.

4.3.1. Bubbles entrained within the liquid slugs and the liquid film around Taylor bubbles

The two peaks in Probability Density Function which occur for slug flow can be identified with the mean void fractions in the liquid slugs and the Taylor bubbles, respectively. The peak at lower void fraction indicates the bubble entrainment in the liquid slug and higher one is related to the film thickness around the Taylor bubble. The values extracted are plotted against mixture velocity in Figs. 17 and 18. Also shown are the predictions from the model proposed by Barnea and Ullmann (2004). For void fraction in the liquid slug, the model works well at liquid superficial velocities <0.4 m/s. But there is an additional effect of liquid flow rate. A similar trend was also observed in the results by Mori and Miwa (2002) for 25.8 mm diameter pipe. Moreover, the void fraction in the Taylor bubble region shows a large spread of data.

4.3.2. Taylor bubble/liquid slug lengths

Individual Taylor bubbles and liquid slugs were identified by applying two thresholds to the time series of void fraction. The positions of the front and tail of Taylor bubbles were detected by the sign change of the slope of time series. Time delay between these points and the velocity derived from Eq. (1) were used to determine the Taylor bubble and liquid slug lengths. Individual value of these lengths vary, therefore, mean values of the distributions obtained are discussed here. The results are shown in Figs. 19 and 20, which show that the Taylor bubble length increases with gas superficial velocity whilst the liquid slug length shows a less systematic trend. A stronger effect of liquid flow rate is seen

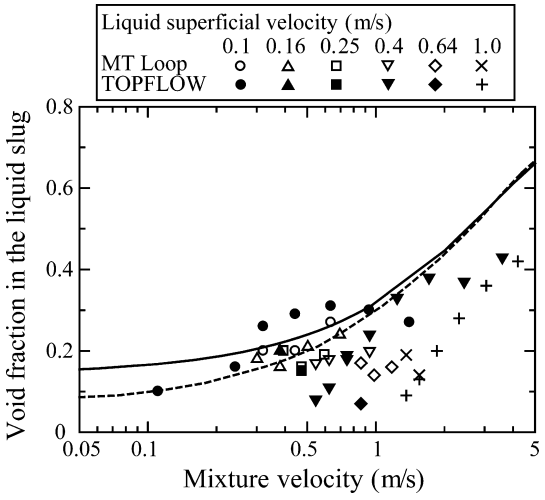

Fig. 17. Void fraction in the liquid slug region against mixture velocity. Model by Barnea and Ullmann (2004). The dashed line is from the version of the model with re-coalescence whilst the solid line is from that version omitting re-coalescence.

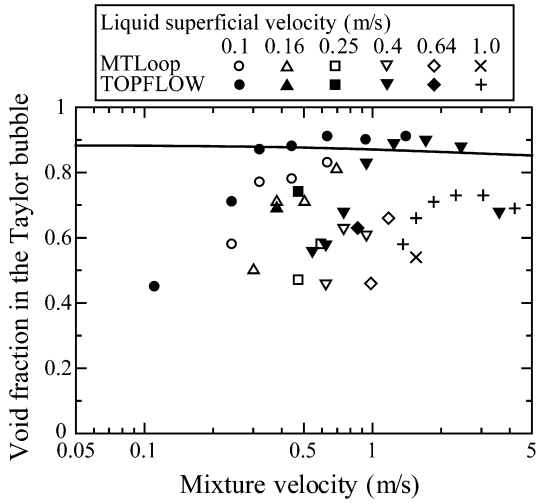

Fig. 18. Void fraction in the Taylor bubble region against mixture velocity (solid line: model by Barnea and Ullmann (2004)).

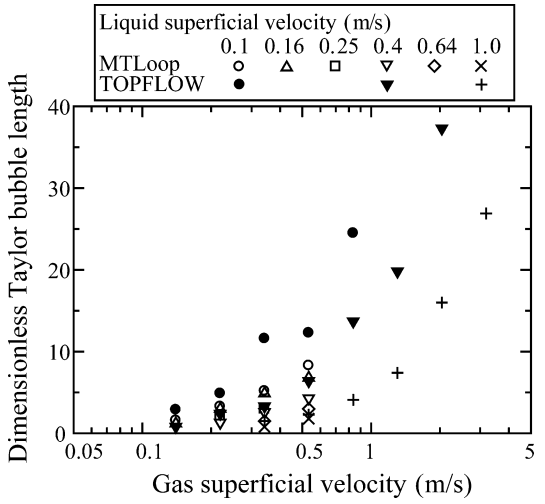

Fig. 19. Average dimensionless Taylor bubble length against gas superficial velocity.

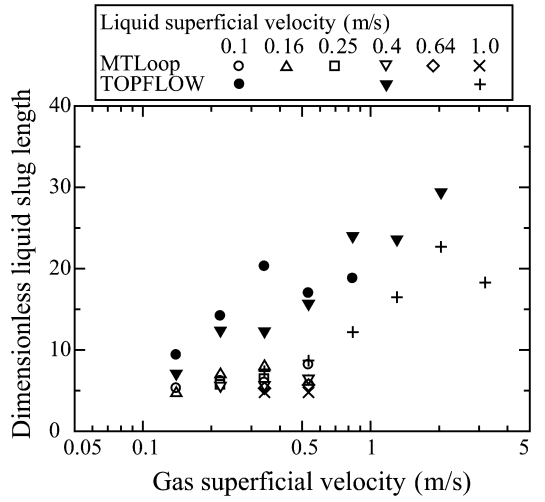

Fig. 20. Average dimensionless liquid slug length against gas superficial velocity.

Table 1
Data bank of Taylor bubble/slug lengths around 50 mm pipe diameter.

Author	Diameter (mm)	Sampling heights (m)	Sensor
Mao and Dukler (1989)	50.8	5.46, 6.68, 8.87	Radio-frequency probe
Mi et al. (2001)	50.8	2.0	Impedance void-meter
van Hout et al. (2002)	54.0	0.91, 2.72. 4.79, 6.86	Optical fibre probe

for the Taylor bubble length than for the liquid slug length. These data were compared with previously published data taken from sources listed in Table 1. Results from Mi et al. (2001) (short pipe lengths) and from van Hout et al. (2002) and Mao and Dukler (1989) (long pipe lengths) are presented in Figs. 21 and 22. Slug velocities were not measured in the present work. Therefore values predicted using Eq. (1) were employed. That equation had been shown to correctly predict velocity data when these were available in the data bank created from sources given in Tables 1 and 2. Only the difference appears at high gas flow rate where the slug to churn transition might occurs. It becomes difficult to identify the Taylor bubble and slug lengths in this region since the time series become irregular. Mi et al. (2001) reported that slug flow is gradually developing, i.e., the Taylor bubble and liquid slug length vary with the axial length. The discrepancies with axial distances for the Taylor bubble length are found to become less with increasing liquid flow rate. In contrast, for the liquid slug length, the variation with axial distances appears more independent of liquid flow rate.

Fig. 23 shows the relationship between the dimensionless liquid slug length and Taylor bubble length. It can be seen that the greater the distance of the measuring point from the inlet, the larger the dimensionless liquid slug length. Note that these results show that the effect of pipe length seems to have ceased by 100 pipe diameters indicating the flow is fully developed. Co-incidentally this is what was identified for bubbly flow by Herringe and Davis (1976). Akagawa et al. (1971) proposed a correlation equation.

$$L_S = \frac{1}{\left(0.001L_B^{0.55} + 0.093L_B^{-0.52}\right)} \tag{8}$$

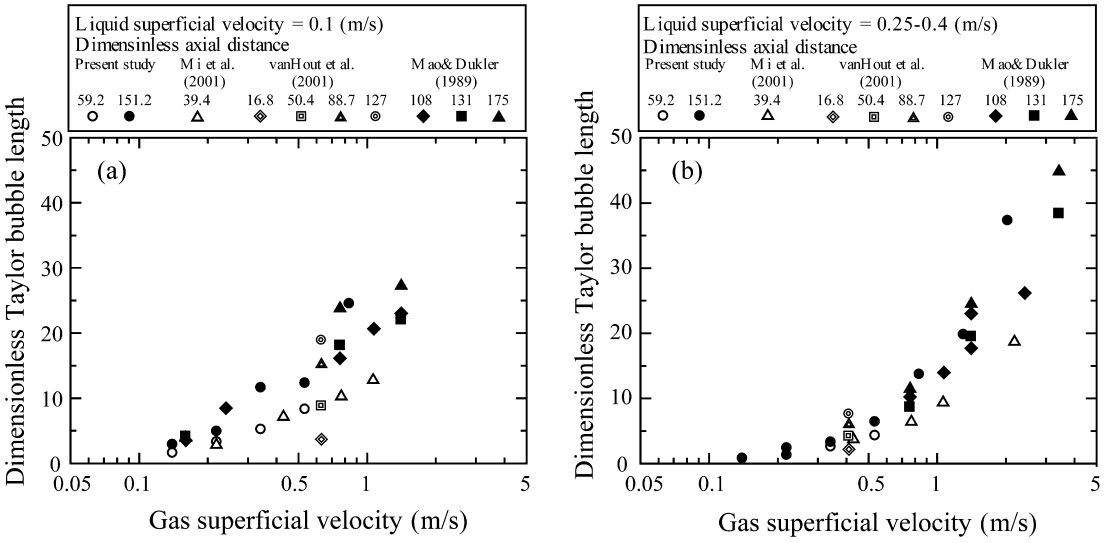

Fig. 21. Comparison of the Taylor bubble length with published data bank for different liquid superficial velocities ((a) 0.1 m/s, (b) 0.25–0.4 m/s).

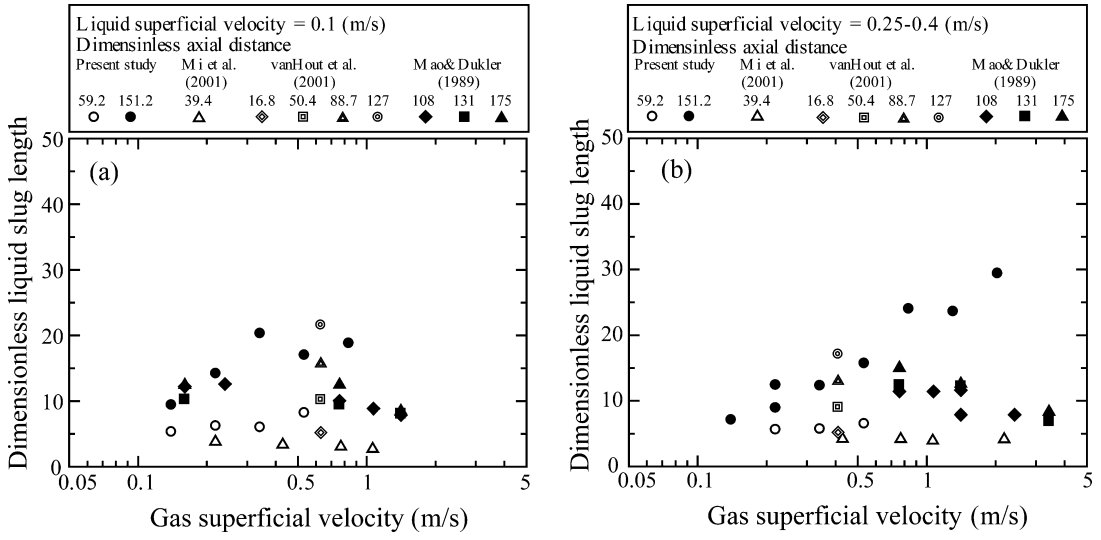

Fig. 22. Comparison of the liquid slug length with published data bank for different liquid superficial velocities ((a) 0.1 m/s, (b) 0.25–0.4 m/s).

Table 2
Data bank of frequency from different pipe diameter.

Author	Pipe diameter (mm)	Sampling heights (m)	Sensor
Omebere-Iyari and Azzopardi (2007)	5.0	2.88	Conductance probe
Kaji et al. (2007)	19.0	5.7	Conductance probe
Hatakeyama et al. (1987)	20.6	3.05	Needle probe
Van Hout et al. (2002)	24.0	6.88	Optical fibre probe
Sekoguchi and Mori (1997)	26.0	5.34	Conductance probe
Akagawa et al. (1971)	27.6	2.6	Needle probe
Cheng et al. (2002)	29.0	3.6	Impedance void-meter
Zheng and Che (2006)	35.0	3.5	Needle probe
Legius et al. (1997)	50.0	14	Light attenuation
Davis and Fungtamasan (1984)	50.8	2.75, 4.66	Needle probe
Kaji et al. (2007)	70.0	6.7	Conductance probe
Cheng et al. (1998)	150.0	7.3	Impedance void-meter

where L_S and L_B are the lengths of the liquid slugs and of the Taylor bubble respectively. Both are in metres. The predictions of this equation are shown in Fig. 23 where they show good agreement with the data from Z/D_t>100. This in spite of having been developed using data from pipes of 27.6 mm diameter, i.e., about half the pipe diameter of the present data set.

4.4. Slug frequencies

4.4.1. The effect of flow development

Fig. 24(a)–(d) show how the frequency varies with the axial distance at different liquid flow rates. A good correlation and a systematic trend are found when Strouhal number based on mixture velocity is plotted against dimensionless axial distance. The frequency decreases as flow travels downstream. Data for u_{ls} <0.25 show little effect of liquid flow rate, therefore these data plotted together. In these figures the results by Legius et al. (1997) from 50 mm diameter pipe are also plotted. These were measured at 14 m (Z/D_t = 140) from the inlet section whose diameter was 80 mm initially then contracted to 50 mm at 7 m height. They agree well with the present data. Overall the Strouhal number

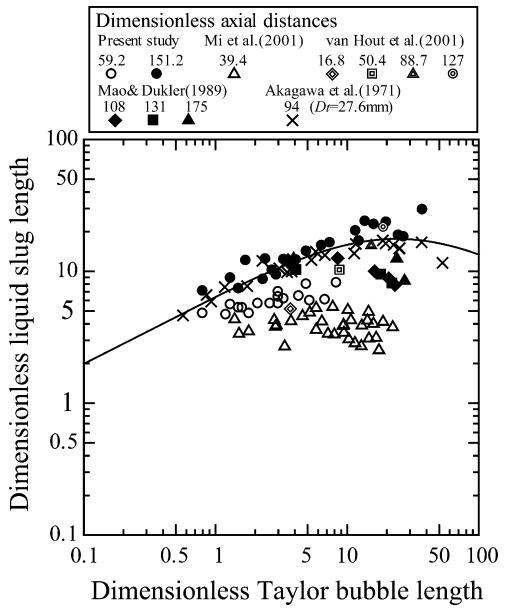

Fig. 23. Effect of dimensionless Taylor bubble length on dimensionless liquid slug length clearly showing how the latter increases with number of pipe diameters from the mixer. The line shows the predictions of the correlation of Akagawa et al. (1971).

based on mixture velocity, u_m, can be represented by the following equation:

$$St_m = \frac{fD_t}{u_m} = AB\left(\frac{Z}{D_t}\right)^{-0.6} \tag{9}$$

where $u_m = u_{gs} + u_{ls}$ and the coefficients A and B are given $A = u_{gs}^{-0.75}$, $B = 0.74u_{ls}+0.53$, respectively. The regression coefficients were all >0.973.

Alternatively a correlation for Strouhal number based on gas superficial velocity was constructed:

$$St_g = \frac{fD_t}{u_{gs}} = CD\left(\frac{Z}{D_t}\right)^{-0.75} \tag{10}$$

where the coefficients C and D are given by $C = u_{gs}^{-1.2}$, $D = 4.94u_{ls}+0.368$, respectively. Again regression coefficients were all >0.97.

Eqs. (9) and (10) and the correlation by Legius et al. (1997) were assessed by using the data bank listed in Table 2. The correlation by Legius et al. (1997) are given by

$$f = 0.0543\frac{u_{ls}}{u_m}\left(\frac{2.02}{D_t}+\frac{u_m^2}{gD_t}\right)^{1.02}. \tag{11}$$

A logarithmic distribution of errors was assumed in quantification of prediction errors proposed by Govan (1988). The error $e(i)$ was defined as,

$$e(i) = \ln\frac{P(i)}{E(i)}, \tag{12}$$

where $P(i)$ and $E(i)$ are the predicted and experimental values, respectively. Mean and Standard Deviation of the error, $\bar{e}$ and s, were transformed to $\exp(\bar{e})$ and $\exp(s) - 1$ which provide values relative to the original distribution $P(i)/E(i)$. Mean error, $\exp(\bar{e})$, close to 1 and lower value of Standard Deviation indicate a better result. The analysis was carried out for 140 points from 50 mm diameter pipes. From Table 3, Eq. (9) is seen to give the best performance.

Slug frequency is reasonably correlated if plotted in the dimensionless form, gas based Strouhal number = fD_t/u_{gs}, against mean void fraction as shown in Fig. 25. The difference between the MTLoop and TOPFLOW data is merely a reflection of the effect of length.

4.4.2. Extension to pipes of different diameters

The frequency correlation was applied to the published data from a range of pipe diameters details of which are listed in Tables 1 and 2. All the sources employed air/water except Zheng and Che (2006) who employed nitrogen and aqueous electrolyte solutions. All the sensors identified as conductance probe and impedance

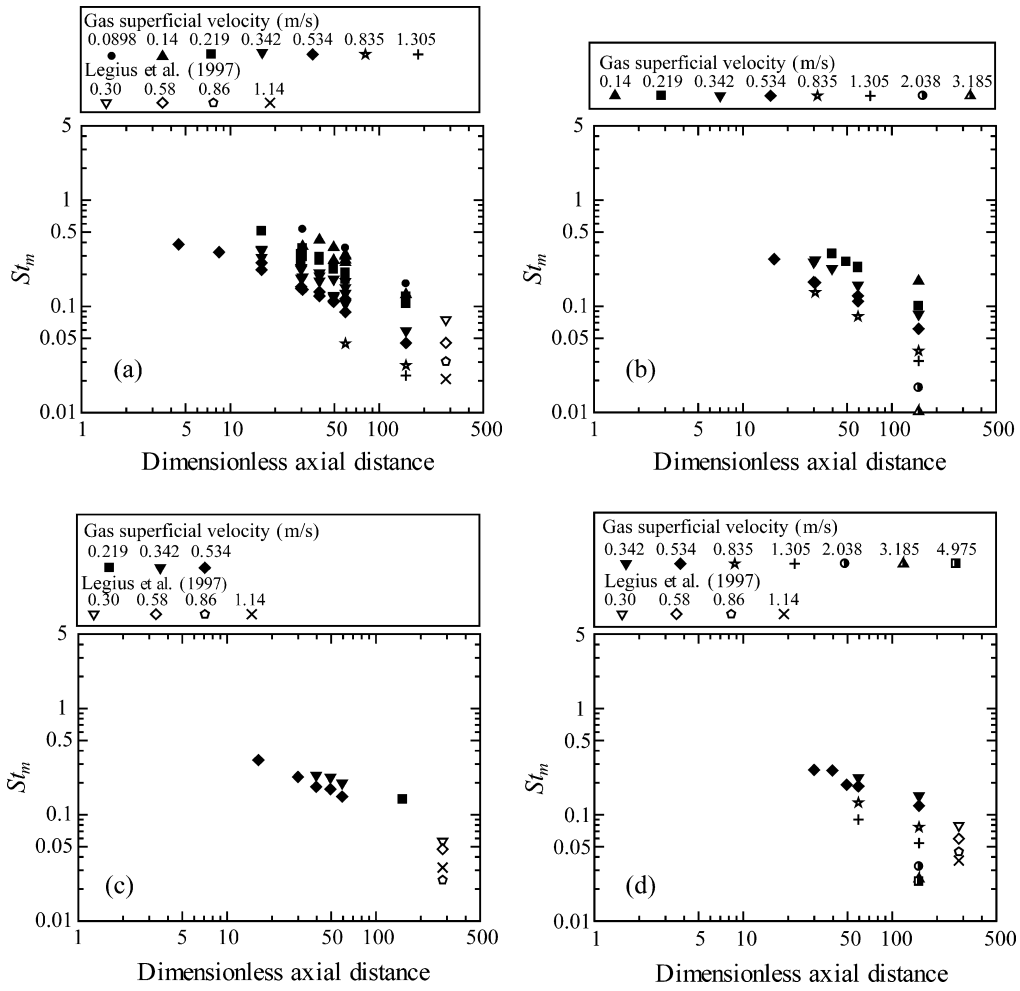

Fig. 24. Variation of Strouhal number based on mixture velocity along the axial distance for different liquid superficial velocities((a) <0.25 m/s, (b) 0.4 m/s, (c) 0.65 m/s, (d) 1.0 m/s).

Table 3
Error analysis of frequency correlations.

Correlation	Mean of error	Standard Deviation
Eq. (9)	0.980	0.247
Eq. (10)	0.973	0.623
Legius et al. (1997)	0.507	1.186

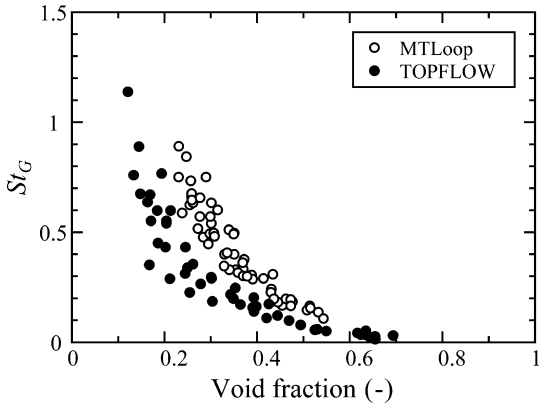

Fig. 25. Strouhal number based on gas superficial velocity against mean void fraction.

void-meter were flush mounted type. Fig. 26 shows the slug frequency predicted using Eq. (9) plotted against measured frequency. Symbols indicate different diameter pipes from sources listed in Tables 1 and 2. The correlation, Eq. (9), gave a reasonable prediction from pipe diameters in the range of 5–150 mm.

The plot of the gas based Strouhal number versus void fraction (Fig. 25) shows different trends for each of the two facilities

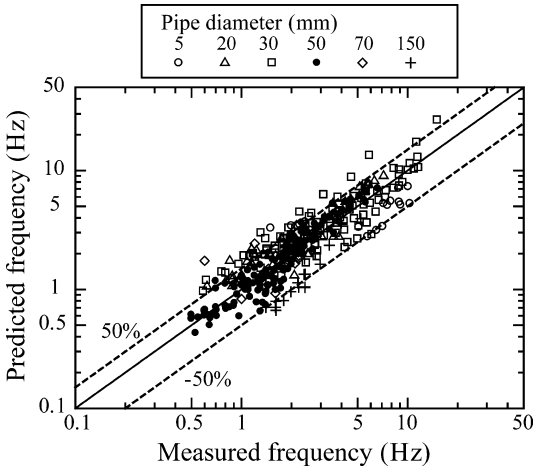

Fig. 26. Measured frequency against predicted frequency using Eq. (9).

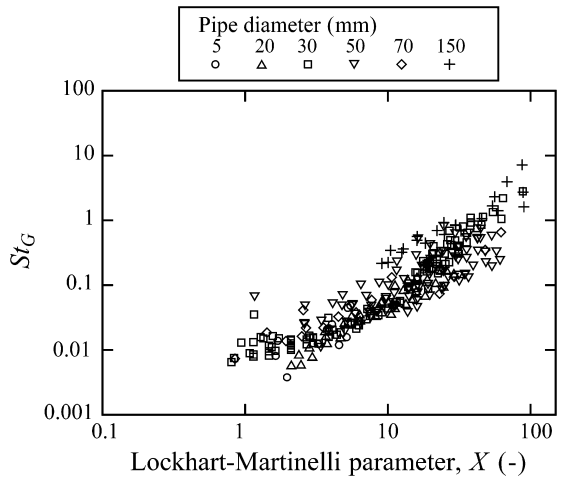

Fig. 27. Strouhal number based on gas superficial velocity against Lockhart–Martinelli parameter.

considered. These and other published data can be seen to be brought together if plotted against the Lockhart–Martinelli parameter, $X = \sqrt{[(dp/dz)_l/(dp/dz)_g]}$, as shown in Fig. 27. In this figure, the results at the lower liquid superficial velocity <0.2 were eliminated which were spread over the shown results. These conditions were considered not to be fully developed. It might be required the longer axial distance to reach the stable state for the condition at lower liquid flow rates.

5. Conclusions

Slug characteristics in vertical upflow have been studied using data from 50 mm diameter pipes together with previously published data. The results were extracted from the time series of cross-sectionally averaged void fraction converted from three dimensional data by using wire mesh sensors. Extensive measurements at different axial distances from the inlet gave the useful information for investigating flow development. The following conclusions were drawn:

1. Flow pattern, void fraction, Taylor bubble/slug lengths, slug frequencies vary with the axial position.
2. The correlation proposed by Lucas et al. (2005) correctly predicts the bubble to slug transition at different axial positions. The idea of using a critical void fraction proposed by Taitel et al. (1980) can be employed. However, higher critical void fractions are required to correctly predict the transitions near the inlet.
3. The statistical analysis shows that Standard Deviation gives a good identification of slug flow whilst others such as Skewness and Kurtosis do not link clearly with flow pattern.
4. The Taylor bubble length increases systematically with gas flow rate but the slug length is less systematic. Both lengths increase as flow travels downstream.
5. Although the Taylor bubble/liquid slug lengths seems to converge at about $100D_t$, the gradual decrease of slug frequency was observed even at the furthest measurement point ($L/D_t = 151.2$). A frequency correlation has been proposed which included the effect of the axial distance. Applying the correlation to the data bank confirmed this correlation works successfully.
6. The data from different diameter pipes are well correlated using the Strouhal number based on gas superficial velocity against the Lockhart–Martinelli parameter.

Acknowledgements

This work was carried out as a collaboration between the University of Nottingham and Forschungszentrum Dresden-Rossendorf e.V. during the two months stay of R. Kaji at Forschungszentrum Dresden-Rossendorf e.V. R. Kaji acknowledges support from Business-Engineering and Science Travel Scholarship (BESTS). The experiments were carried out in the frame of two research projects funded by the German Federal Ministry of Economics and Labour, project numbers 150 1215 and 150 1265.

Appendix A. Definitions of statistical parameters

The standard deviation of a time series can be defined as

$$\sigma = \frac{\sum_{i=1}^{n}(\varepsilon_{gi} - \bar{\varepsilon}_g)^2}{n} \tag{A1}$$

The Skewness is given by

$$Sk = \frac{\frac{1}{n}\sum_{i=1}^{n}(\varepsilon_{gi} - \bar{\varepsilon}_g)^3}{\sigma^3} \tag{A2}$$

whilst the Kurtosis is

$$Ku = \frac{\frac{1}{n}\sum_{i=1}^{n}(\varepsilon_{gi} - \bar{\varepsilon}_g)^4}{\sigma^4} \tag{A3}$$

In this ε_{gi} is the cross-sectionally averaged void fraction at time t_i, $\bar{\varepsilon}_g$, is the time averaged void fraction and n is the number of samples in the time series.

References

Akagawa, K., Hamaguchi, H., Sakaguchi, T., 1971. Studies on the fluctuation of pressure drop in two-phase slug flow. Bull. JSME 14, 462–469.
Azzopardi, B.J., 2006. Gas Liquid Flows. Begell House Inc., New York.
Barnea, D., Ullmann, A., 2004. Modelling of gas entrainment from Taylor bubbles. Part A: Slug flow. Int. J. Multiphase Flow 30, 239–272.
Brown, D.J., Jensen, A., Whalley, P.B., 1975. Non-equilibrium effects in heated and unheated annular two-phase flow. ASME Paper 75-WA/HT/7.
Cheng, H., Hills, J.H., Azzopardi, B.J., 1998. A study of the bubble-to-slug transition in vertical gas–liquid flow in columns of different diameter. Int. J. Multiphase Flow 24, 431–452.
Cheng, H., Hills, J.H., Azzopardi, B.J., 2002. Effects of initial bubble size on flow pattern transition in a 28.9 mm diameter column. Int. J. Multiphase Flow 28, 1047–1062.
Chisholm, D., 1972. An equation for velocity ratio in two-phase flow. NEL Report No 535.
Costigan, G., Whalley, P.B., 1996. Slug flow regime identification from dynamic void fraction measurements in vertical air–water flows. Int. J. Multiphase Flow 23, 228–263.
Davis, M.R., Fungtamasan, B., 1984. Large scale structures in gas–liquid mixture flows. Int. J. Multiphase Flow 6, 663–676.
Delfos, R., Wisse, C.J., Oliemans, R.V.A., 2001. Measurements of air entrainment from a stationary Taylor bubble in a vertical tube. Int. J. Multiphase Flow 27, 1769–1787.
Fabre, J., Liné, A., 1992. Modeling of two-phase slug flow. Annu. Rev. Fluid Mechanics 24, 21–46.
Fernandes, R.C., Semiat, R., Dukler, A.E., 1983. Hydrodynamic model for gas–liquid slug flow in vertical tubes. AIChE J. 29, 981–989.
Govan, A.H., 1988. A note on statistical methods for comparing measured and calculated values. UKAEA Report AERE-M3621.
Guet, S., Ooms, G., Oliemans, R.V.A., 2002. Influence of bubble size on the transition from low-Re bubbly flow to slug flow in a vertical pipe. Exp. Thermal Fluid Sci. 26, 635–641.
Hatakeyama, N., Noda, K., Kawashima, T., 1987. Studies on two-phase gas–liquid flow in vertical pipes (4th Report). J. Mining Metallurg. 103, 785–791.
Herringe, R.A., Davis, M.R., 1976. Structural development of gas–liquid mixture flows. J. Fluid Mech. 73, 97–123.
Heywood, N.I., Richardson, J.F., 1979. Slug flow of air–water mixtures in a horizontal pipe: determination of liquid holdup by gamma-ray absorption. Chem. Eng. Sci. 34, 17–30.
Jayanti, S., Hewitt, G.F., 1992. Prediction of the slug-to-churn transition in vertical two-phase flow. Int. J. Multiphase Flow 18, 847–860.
Jones, O.C., Zuber, N., 1975. The interrelation between void fractions and flow patterns in two-phase flow. Int. J. Multiphase Flow 2, 3, 273–306.
Kaji, R., Omebere-Iyari, N.K., Hernandez Perez, V., Azzopardi, B.J., 2007. The effect of pipe diameter on flow patterns in vertical upflow. In: Sixth International Conference on Multiphase Flow CD-ROM, #000.

Legius, H.J.W.M., van den Akker, H.E.A., Narumo, T., 1997. Measurements on wave propagation and bubble and slug velocities in cocurrent upward two-phase flow. Exp. Thermal Fluid Sci. 15, 267–278.

Liu, T.J., 1993. Bubble size and entrance length effects on void development in a vertical channel. Int. J. Multiphase Flow 19, 99–113.

Lucas, D., Krepper, E., Prasser, H.-M., 2003. Evolution of flow patterns, gas fraction profiles and bubble size distributions in gas–liquid flows in vertical tubes. Trans. Inst. Fluid-Flow Mach. 112, 37–46.

Lucas, D., Krepper, E., Prasser, H.-M., 2005. Development of co-current air–water flow in a vertical pipe. Int. J. Multiphase Flow 31, 1304–1328.

Mao, Z.-S., Dukler, A.E., 1989. An experimental study of gas–liquid slug flow. Exp. Fluids 8, 169–182.

Mi, Y., Ishii, M., Tsoukalas, L.H., 2001. Investigation of vertical slug flow with advanced two-phase flow instrument. Nucl. Eng. Design 204, 69–85.

Moissis, R., Griffith, P., 1962. Entrance effects in a two-phase slug flow. J. Heat Transfer 84, 29–39.

Mori, K., Miwa, M., 2002. Structure and void fraction in a liquid slug for gas–liquid two-phase slug flow. Heat Transfer Asian Res. 31, 257–271.

Nicklin, D.J., Wilkes, J.O., Davidson, J.F., 1962. Two-phase flow in vertical tubes. Trans. Inst. Chem. Eng. 40, 61–68.

Omebere-Iyari, N.K., Azzopardi, B.J., 2007. A study of flow patterns for gas/liquid flow in small diameter tubes. Chem. Eng. Res. Design 85, 1–13.

Pinto, A.M.F.R., Campos, J.B.L.M., 1996. Coalescence of two gas slugs rising in a vertical column of liquid. Chem. Eng. Sci. 51, 45–54.

Prasser, H.-M., Böttger, A., Zschau, J., 1998. A new electrode-mesh tomograph for gas–liquid flows. Flow Measure. Instrument. 9, 111–119.

Prasser, H.-M., Scholz, D., Zippe, C., 2001. Bubble size measurement using wire-mesh sensors. Flow Measure. Instrument. 12, 299–312.

Prasser, H.-M., Beyer, M., Carl, H., Gregor, S., Lucas, D., Pietruske, H., Schütz, P., Weiss, F.-P., 2007. Evolution of the structure of a gas–liquid two-phase flow in a large vertical pipe. Nucl. Eng. Design 237, 1848–1861.

Radovcich, N.A., Moissis, R., 1962. The transition from two-phase bubble flow to slug flow. MIT Report No. 7-7673-22.

Sekoguchi, K., Mori, K., 1997. New development of experimental study on interfacial structure in gas–liquid two-phase flow. Exp. Heat Transfer Fluid Mech. Thermodynamics 2, 1177–1188.

Song, C.H., No, H.C., Chung, M.K., 1995. Investigation of bubble flow developments and its transition based on the instability of void fraction waves. Int. J. Multiphase Flow 21, 381–404.

Sylvester, N.D., 1987. A mechanistic model for two-phase vertical slug flow in pipes. Trans. ASME 109, 206–213.

Taitel, Y., Bornea, D., Dukler, A.E., 1980. Modelling flow pattern transitions for steady upward gas–liquid flow in vertical tubes. AIChE J. 26, 345–354.

Taitel, Y., Dukler, A.E., 1976. A model for predicting flow regime transitions in horizontal and near horizontal pipes. Int. J. Multiphase Flow 22, 47–55.

van Hout, R., Barnea, D., Shemer, L., 2001. Evolution of statistical parameters of gas–liquid flow along vertical pipes. Int. J. Multiphase Flow 27, 1579–1602.

van Hout, R., Barnea, D., Shemer, L., 2002. Translational velocities of elongated bubbles in continuous slug flow. Int. J. Multiphase Flow 28, 1333–1350.

Wolf, A., Jayanti, S., Hewitt, G.F., 2001. Flow development in vertical annular flow. Chem. Eng. Sci. 56, 3221–3235.

Zabaras, G.J., 2000. Prediction of slug frequency for gas/liquid flows. SPE J. 5, 252–258.

Zheng, D., Che, D., 2006. Experimental study on hydrodynamic characteristics of upward gas–liquid slug flow. Int. J. Multiphase Flow 32, 1191–1218.